Preprints of the 8th IFAC International Conference on Manoeuvring and Control of Marine Craft, September 16-18, 2009
Casa Grande Hotel, Guarujá (SP), Brazil

Posterior Cramér-Rao bounds analysis for INS/USBL navigation systems

M. Morgado P. Oliveira C. Silvestre [1]

IST - Instituto Superior Técnico
ISR - Institute for Systems and Robotics
Av. Rovisco Pais, 1, 1049-001, Lisbon, Portugal
{marcomorgado,pjcro,cjs}@isr.ist.utl.pt

Abstract: This paper presents a performance analysis for Ultra-Short Base Line (USBL) aided Inertial Navigation Systems (INS) resorting to lower bounds for the covariance of the estimators based on the Posterior Cramér-Rao Bounds (PCRB) theory. In this framework, the vehicle interrogates acoustic transponders located in known positions of the mission area. Two distinct design methodologies are presented: one that estimates essentially the position of the origin of the Body attached coordinate frame with respect to Earth, and the latter that tracks the position of the transponders in the Body-fixed coordinate frame. The performance of both systems is compared in simulation leading to the conclusion that it is equivalent. Their efficiency is also assessed in simulation by verifying that both systems perform near the PCRB.

1. INTRODUCTION

In recent years, low-cost Inertial Navigation Systems (INS) stepped forward as a significant aid for Underwater Vehicles (UV) positioning in the fulfillment of several missions at sea. The execution of these tasks, that include environmental monitoring, surveillance, underwater inspection of estuaries, harbors, and pipelines, and geological and biological surveys (see Pascoal et al. [2000]), requires low-cost, compact, high performance, and robust navigation systems that can accurately estimate the UV position and attitude. The average INS yields excellent short-term accuracy, however, long term position drifts arise due to the integration of non-ideal inertial sensors bias and noise, if not compensated by external aiding sensors.

Among several available underwater navigation aiding sensors such as Doppler Velocity Loggers (DVL), depth pressure sensors, and magnetic compasses, acoustic positioning systems (see Milne [1983], and Vickery [1998]) like Long Base Line (LBL), Short Base Line (SBL), and Ultra-Short Base Line (USBL) stand often as the primary choice for underwater positioning (see Lurton and Millard [1994], Smith and Kronen [1997], Larsen [2000], and Lee et al. [2004]).

In the proposed mission scenarios, illustrated in Fig. 1, the vehicle is equipped with an INS and an USBL array, in an inverted USBL configuration (Vickery [1998]), that interrogates transponders located in known positions of the mission area, engaging in interrogations over considerable distances, ranging typically from a few meters to several kilometers.

Theoretical performance bounds have long been pursued as an important design tool that helps gauge the attainable performance by any estimator on preset conditions of process observations and noise. These kind of bounds allow as well for an assessment of whether imposed performance specifications are feasible or not. A commonly used lower bound for time-invariant statistical models is the Cramér-Rao bound (CRB) which provides a lower bound on the estimation error of any estimator of an unknown constant parameter of that particular statistical model. An analogous bound for random parameters on non-linear, non-stationary system models was first derived in Van Trees [1968], and is referred to as the Posterior Cramér-Rao Bound (PCRB), which is used in the work presented in this paper to assess the achievable performance of the navigation systems.

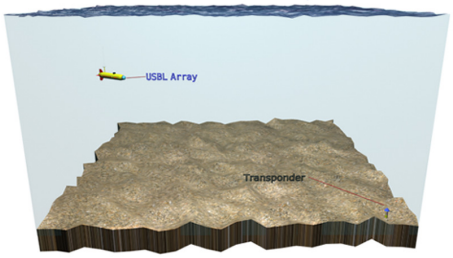

Fig. 1. Mission scenario

Control systems for this type of robotic vehicles often rely on information provided by external observers to feedback errors and steer the vehicle to its desired pose. The choice of where this quantities (e.g. position, velocity, and attitude) are expressed, either on Body or Earth fixed coordinate frames, depends on the purpose, application and mainly on the design methodology of the controller.

The navigation system can be designed to provide estimates expressed on any specific coordinate frame, either by posterior conversion of the outputs from one frame to another (e.g. estimator designed to provide outputs on Earth fixed coordinates with posterior conversion to Body fixed coordinates or vice-versa) or by directly designing the systems on the desired coordinate frame. Intuitively one might expect each coordinate frame tailored filter to perform better then the other on its own design frame due, for instance, to unaccounted posterior frame con-

[1] This work was partially supported by Fundação para a Ciência e a Tecnologia (ISR/IST plurianual funding) through the POS_Conhecimento Program that includes FEDER funds and by the project PDCT/MAR/55609/2004 - RUMOS of the FCT. The work of M. Morgado was supported by PhD Student Scholarship SFRH/BD/25368/2005 from the Portuguese FCT POCTI programme.

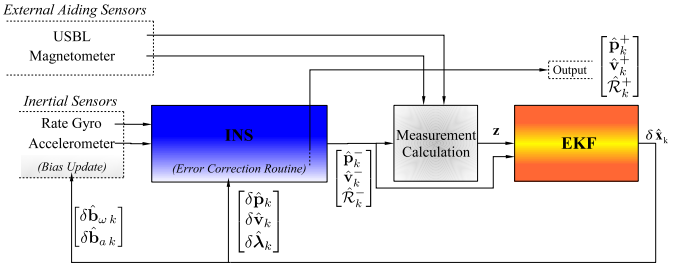

Fig. 2. Navigation system block diagram

version during the filtering process. Moreover, most inertial quantities are directly sensed on Body coordinate frame, whereas for use on an Earth frame designed system these have to be correctly converted from Body to Earth coordinates. Positioning devices aboard the vehicle like inverted USBL configurations obtain directly the position of transponders in Body-fixed coordinates motivating the use of Body referenced estimators.

The work presented herein shows, resorting to Monte-Carlo simulations, that for this class of navigation systems the overall performance of the estimators is equivalent and also asserts that both estimators perform closely to the expected theoretical lower bound, emphasizing their efficiency and leaving little margin for improvement. To the best knowledge of the authors, this paper presents for the first time the application of PCRB tools on this kind of estimators, set on a framework of a direct-feedback EKF estimating and correcting errors on an INS. This paper also presents two estimators: one designed to estimate the position and velocity of the Body frame in Earth fixed coordinates, while the other is designed to estimate the position of the interrogated transponder in the Body frame and Body velocity with respect to Earth expressed in Body-fixed coordinates.

The paper is organized as follows: the main aspects and the proposed architecture of the navigation systems synthesized on both designated Body and Earth fixed coordinate frames, are reviewed in Section 2. Section 2 also gives a brief review on the USBL positioning system and the fusion techniques to aid the inertial navigation systems. The theory behind the PCRB and the method on how to compute it is presented in Section 3. Section 4 presents the simulation results that validate the proposed techniques and compares the performance of both systems against each other and against the PCRB. Finally Section 5 provides some conclusion remarks and comments on future work.

2. NAVIGATION SYSTEM ARCHITECTURE

The proposed navigation system architecture is depicted in Fig. 2. The INS is the backbone algorithm that performs attitude, velocity and position numerical integration from rate gyro and accelerometer triads data, rigidly mounted on the vehicle structure (strapdown configuration). The undesirable INS estimates drift, due to integration of non ideal inertial sensor disturbances (bias and noise), is dynamically compensated by the EKF that estimates position, velocity, attitude and bias compensation errors, according to the direct-feedback configuration shown in Fig. 2. After the error correction procedure is completed, the EKF error estimates are reset maintaining the filter linearization assumptions valid.

The inputs provided to the inertial algorithms are the accelerometer and rate gyro readings, corrupted by zero mean white Gaussian noise $\mathbf{n}$ and random walk bias, $\dot{\bar{\mathbf{b}}} = \mathbf{n}_b$, yielding

$$ {}^{B}\mathbf{a}_{SF} = {}^{B}\bar{\mathbf{a}} + {}^{B}\bar{\mathbf{g}} - \delta\mathbf{b}_a + \mathbf{n}_a, \quad \boldsymbol{\omega} = \bar{\boldsymbol{\omega}} - \delta\mathbf{b}_\omega + \mathbf{n}_\omega $$

where $\delta\mathbf{b} = \mathbf{b} - \bar{\mathbf{b}}$ denotes bias compensation error, $\bar{\mathbf{b}}$ is the nominal bias, $\mathbf{b}$ is the compensated bias, ${}^{B}\bar{\mathbf{g}}$ is the nominal gravity vector, and the subscripts a and ω identify accelerometer and rate gyro quantities, respectively.

2.1 Attitude algorithm

The attitude of the vehicle is defined to be the orientation of the Body coordinate frame with respect to a Earth fixed coordinate frame. It can be expressed by a rotation matrix $\mathcal{R} \in SO(3)$, which represents a rotation from Body to Earth fixed coordinate frame, with kinematics given by

$$ \dot{\mathcal{R}} = \mathcal{R}[\omega\times] \tag{1} $$

where ω is the angular velocity of the Body frame with respect to Earth, expressed in Body coordinates. Both formulations of the navigation system presented in this work share the same attitude representation and computations.

For highly maneuverable vehicles, the attitude numerical integration algorithm must properly address angular high-frequency motions (coning) to avoid attitude estimation errors build-up. The attitude multi-rate approach, based on the work detailed in Savage [1998a], computes the dynamic angular rate effects using high-speed, low order algorithms, whose output is periodically fed to a moderate-speed algorithm that computes attitude resorting to exact, closed-form equations. Discrete time Body fixed frame attitude updates are computed in Direction Cosine Matrix (DCM) form

$$ {}^{B_{k-1}}_{B_k}\mathbf{R}(\boldsymbol{\lambda}_k) = \mathbf{I}_{3\times3} + \frac{\sin\|\boldsymbol{\lambda}_k\|}{\|\boldsymbol{\lambda}_k\|}[\boldsymbol{\lambda}_k\times] + \frac{1-\cos\|\boldsymbol{\lambda}_k\|}{\|\boldsymbol{\lambda}_k\|^2}[\boldsymbol{\lambda}_k\times]^2 \tag{2} $$

where $\|\cdot\|$ represents the Euclidean norm, $\{B_k\}$ is the Body frame at time k and ${}^{B_{k-1}}_{B_k}\mathbf{R}(\boldsymbol{\lambda}_k)$ is the rotation matrix from $\{B_k\}$ to $\{B_{k-1}\}$ coordinate frames, parameterized by the rotation vector $\boldsymbol{\lambda}_k$. The rotation vector updates are formulated as $\boldsymbol{\lambda}_k = \boldsymbol{\alpha}_k + \boldsymbol{\beta}_k$ in order to denote angular integration and coning attitude terms $\boldsymbol{\alpha}_k$ and $\boldsymbol{\beta}_k$, respectively. The attitude high-speed algorithm computes $\boldsymbol{\beta}_k$ as a summation of the high-frequency angular rate vector changes using simple, recursive computations (Savage [1998a]), providing high-accuracy results.

The attitude error equation, implemented in the EKF, was brought to full detail by Britting [1971] and models the attitude error dynamics

$$ \delta\dot{\boldsymbol{\lambda}} = -\mathcal{R}\delta\mathbf{b}_\omega + \mathcal{R}\mathbf{n}_\omega \tag{3} $$

respectively, where the attitude error rotation vector $\delta\boldsymbol{\lambda}$ is defined by $\mathbf{R}(\delta\boldsymbol{\lambda}) = \mathcal{R}\bar{\mathcal{R}}^T$, bearing a first order approximation

$$ \mathbf{R}(\delta\boldsymbol{\lambda}) \simeq \mathbf{I}_{3\times3} + [\delta\boldsymbol{\lambda}\times] \Rightarrow [\delta\boldsymbol{\lambda}\times] \simeq \mathcal{R}\bar{\mathcal{R}}^T - \mathbf{I}_{3\times3} \tag{4} $$

of the Direction Cosine Matrix (DCM) parametrization, where $\bar{\mathcal{R}}$ represents nominal rotation matrix.

The INS attitude estimate, $\mathcal{R}_k^-$, is compensated in the INS error correction routines as depicted in Fig. 2, using the rotation error matrix $\mathbf{R}(\delta\boldsymbol{\lambda})$ definition, which yields

$$ \mathcal{R}_k^+ = \mathbf{R}_k^T(\delta\hat{\boldsymbol{\lambda}}_k)\mathcal{R}_k^- $$

where $\mathbf{R}_k^T(\delta\hat{\boldsymbol{\lambda}}_k)$ is parameterized by the rotation vector $\delta\hat{\boldsymbol{\lambda}}_k$ according to the DCM form.

2.2 Earth-fixed position and velocity computation

In the Earth-fixed proposed solution, the navigation system estimates the position and velocity of the Body coordinate frame with respect to an Earth fixed coordinate frame, both represented in Earth coordinates. The discrete numerical integration scheme computes solutions at fixed discrete times for the simplified continuous dynamics

$$ {}^{E}\dot{\mathbf{p}} = {}^{E}\mathbf{v} \tag{5} $$

$$ {}^{E}\dot{\mathbf{v}} = \mathcal{R}^{B}\mathbf{a}_{SF} + {}^{E}\,\mathbf{g} \tag{6} $$

where ${}^{E}\mathbf{g}$ represents the gravity vector on Earth, ${}^{E}\dot{\mathbf{v}}$ is the velocity of the origin of the Body frame with respect to Earth, and ${}^{E}\dot{\mathbf{p}}$ is the position of the origin of the Body frame with respect to Earth.

Using the equivalence between strapdown attitude and velocity/position algorithms Roscoe [2001], the same multi-rate approach is applied (Savage [1998b]) to compute exact velocity updates at moderate-speed

$$ \mathbf{v}_k = \mathbf{v}_{k-1} + {}^{E}_{B_{k-1}}\mathbf{R}\Delta\mathbf{v}_k + \Delta\mathbf{v}_{G/Cor\ k} $$

where $\Delta\mathbf{v}_k$ is the velocity increment related to the specific force, and $\Delta\mathbf{v}_{G/Cor\ k}$ represents the velocity increment due to gravity and Coriolis effects Savage [1998b]. The term $\Delta^{B_{k-1}}\mathbf{v}_{SF\ k}$ also accounts for high-speed velocity rotation and high-frequency dynamic variations due to angular rate vector rotation, yielding

$$ \Delta\mathbf{v}_k = \boldsymbol{\upsilon}_k + \Delta\mathbf{v}_{rot\ k} + \Delta\mathbf{v}_{scul\ k} $$

where $\Delta\mathbf{v}_{rot\ k}$ and $\Delta\mathbf{v}_{scul\ k}$ are the rotation and sculling velocity increments respectively, computed by the high-frequency algorithms.

Position updates also account for position rotation compensation and scrolling effects yielding an overall high-accuracy integration algorithm. Readers not familiarized with INS algorithms are referred to Savage [1998a,b], Britting [1971] for further details.

The linear velocity and position errors are defined by

$$ \delta\mathbf{v} = {}^{E}\,\mathbf{v} - {}^{E}\,\bar{\mathbf{v}}\ ,\ \delta\mathbf{p} = {}^{E}\,\mathbf{p} - {}^{E}\,\bar{\mathbf{p}}, \tag{7} $$

respectively, where ${}^{E}\bar{\mathbf{p}}$ is Body frame origin position relative to the Earth coordinate frame, ${}^{E}\mathbf{p}$ the Body frame origin position estimate, ${}^{E}\bar{\mathbf{v}}$ is the nominal linear velocity, and ${}^{E}\mathbf{v}$ the linear velocity estimate.

The linear equation errors are implemented in the EKF, based on the perturbations previously defined in (7), bearing a first-order error model

$$ \dot{\delta\mathbf{p}} = \delta\mathbf{v}\ ,\ \dot{\delta\mathbf{v}} = -\mathcal{R}\delta\mathbf{b}_a - [\mathcal{R}^{B}\mathbf{a}_{SF}\times]\delta\boldsymbol{\lambda} + \mathcal{R}\mathbf{n}_a \tag{8} $$

which are linearly compensated in the INS correction routines using

$$ \mathbf{p}^{+}_{k} = \mathbf{p}^{-}_{k} - \delta\hat{\mathbf{p}}_k\ ,\ \mathbf{v}^{+}_{k} = \mathbf{v}^{-}_{k} - \delta\hat{\mathbf{v}}_k $$

2.3 Body-fixed position and velocity computation

In order to fully exploit the information of the USBL positioning device, the Body-fixed estimator keeps track of the position of the transponder being interrogated in Body coordinates. This allows for an optimal fusion of the position fixes and the transponder position estimates, without any need of transforming between Earth estimates and Body coordinates.

The velocity of the origin of the Body frame with respect to Earth represented in Body-fixed coordinates, is related to the same quantity in Earth-fixed coordinates by

$$ {}^{B}\mathbf{v} = \mathcal{R}^{TE}\mathbf{v} \tag{9} $$

Taking the time-derivative of (9) yields

$$ {}^{B}\dot{\mathbf{v}} = \dot{\mathcal{R}}^{TE}\mathbf{v} + \mathcal{R}^{TE}\dot{\mathbf{v}} \tag{10} $$

Using the rotation matrix kinematics (1) and Earth velocity kinematics in (6) yields

$$ {}^{B}\dot{\mathbf{v}} = {}^{B}\,\mathbf{a}_{SF} + \mathcal{R}^{TE}\mathbf{g} - [\boldsymbol{\omega}\times]^{B}\,\mathbf{v} \tag{11} $$

The position of the transponder on Body frame is given by

$$ {}^{B}\mathbf{p}_t = \mathcal{R}^{T}({}^{E}\mathbf{p}_t - {}^{E}\,\mathbf{p}) \tag{12} $$

where ${}^{E}\mathbf{p}_t$ is the transponder position in Earth coordinates, and ${}^{E}\mathbf{p}$ is the position of the origin of the Body frame in Earth coordinates.

Taking the time-derivative of (12) yields

$$ {}^{B}\dot{\mathbf{p}}_t = \dot{\mathcal{R}}^{T}({}^{E}\mathbf{p}_t - {}^{E}\,\mathbf{p}) + \mathcal{R}^{T}({}^{E}\dot{\mathbf{p}}_t - {}^{E}\,\dot{\mathbf{p}}) \tag{13} $$

Assuming that the transponder is fixed on Earth coordinates (e.g. moored to the sea bottom), thus ${}^{E}\dot{\mathbf{p}}_t = 0$, and using the rotation matrix kinematics (1) comes

$$ {}^{B}\dot{\mathbf{p}}_t = -[\boldsymbol{\omega}\times]^{B}\,\mathbf{p}_t - {}^{B}\,\mathbf{v} \tag{14} $$

The discrete-time solutions for the continuous rigid body dynamics are obtained using an implicit trapezoidal integrator, i.e. second order Adams-Moulton Method (Hairer et al. [1993])

$$ \begin{aligned} g_{v\,k} &= {}^{B}\mathbf{a}_{SF\,k} + \mathcal{R}^{TE}_{k}\mathbf{g} - [\boldsymbol{\omega}_k\times]^{B}\,\mathbf{v}_k \\ {}^{B}\mathbf{v}_k &= {}^{B}\mathbf{v}_{k-1} + \frac{T_k}{2}\left(g_{v\,k} + g_{v\,k-1}\right) \\ g_{p\,k} &= {}^{B}\mathbf{v}_k - [\boldsymbol{\omega}_k\times]^{B}\,\mathbf{p}_{t\,k} \\ {}^{B}\mathbf{p}_{t\,k} &= {}^{B}\mathbf{p}_{t\,k-1} + \frac{T_k}{2}\left(g_{p\,k} + g_{p\,k-1}\right) \end{aligned} $$

where T_k is the sampling interval of the inertial sensors, and the subscript k denotes the sample time index of the estimates and sensor samples. Notice that as it is an implicit algorithm without a closed-form solution, a numeric technique like the Fixed-Point method should be executed in each integration step. Interestingly enough, preliminary assessment tests in a simulation environment showed that the short-term numerical precision of this integration system is equivalent to the high-precision inertial algorithm presented previously.

The Body velocity and position errors are defined similarly to the Earth-fixed case yielding

$$ \delta\mathbf{v} = {}^{B}\,\mathbf{v} - {}^{B}\,\bar{\mathbf{v}}\ ,\ \delta\mathbf{p} = {}^{B}\,\mathbf{p}_t - {}^{B}\,\bar{\mathbf{p}}_t, \tag{15} $$

A first-order perturbation analysis of the continuous kinematics of the Body-fixed system, using the errors defined in (15), then leads to the error model given by

$$ \begin{aligned} \dot{\delta\mathbf{p}} &= -[\boldsymbol{\omega}\times]\,\delta\mathbf{p} - \delta\mathbf{v} - \left[{}^{B}\mathbf{p}_t\times\right]\delta\mathbf{b}_\omega + \left[{}^{B}\mathbf{p}_t\times\right]\mathbf{n}_{b_\omega} \\ \dot{\delta\mathbf{v}} &= -[\boldsymbol{\omega}\times]\,\delta\mathbf{v} + \mathcal{R}^{T}\left[{}^{E}\mathbf{g}\times\right]\delta\boldsymbol{\lambda} - \delta\mathbf{b}_a \\ &\quad - \left[{}^{B}\mathbf{v}\times\right]\delta\mathbf{b}_\omega + \left[{}^{B}\mathbf{v}\times\right]\mathbf{n}_\omega + \mathbf{n}_a \end{aligned} \tag{16} $$

2.4 Bias compensation

The accelerometer and rate gyro bias terms are expressed in the Body frame and modeled in the EKF by

$$ \dot{\delta\mathbf{b}}_\omega = -\mathbf{n}_{b_\omega}\ ,\ \dot{\delta\mathbf{b}}_a = -\mathbf{n}_{b_a} \tag{17} $$

and are linearly compensated in the INS correction routines using

$$ \mathbf{b}^{+}_{a\ k} = \mathbf{b}^{-}_{a\ k} - \delta\hat{\mathbf{b}}_{a\ k}\ ,\ \mathbf{b}^{+}_{\omega\ k} = \mathbf{b}^{-}_{\omega\ k} - \delta\hat{\mathbf{b}}_{\omega\ k} $$

2.5 USBL positioning system and aiding

The USBL sensor consists of a small and compact array of acoustic transducers that allows for the computation of a transponder position in the vehicle coordinate frame, based on the travel time of acoustic signals emitted by the transponder. The measurements provided by these systems have very low update rates (typically below 1 Hz) imposed by physical limitations and mission specific constraints (velocity of acoustic waves in the water, multi-path phenomena, and other disturbances), with a performance that degrades as the transponder/USBL distance increases.

The measurement of travel time is obtained from the round trip travel time of the acoustic signals between the USBL array and the transponder. Taking into account the quantization performed by the acoustic system, the travel time measurements for receiver i are given by

$$t_i = T_s \left[\frac{\bar{t}_i + \varepsilon_c}{T_s} \right] \tag{18}$$

where $\bar{t}_i$ is the nominal travel time, ε_c represents the common mode noise for transponder j (common to all receivers - includes transponder-receiver relative motion time-scaling effects and errors in sound propagation velocity), T_s is the acoustic sampling period and $[\cdot]$ represents the mathematical *round* operator. The travel time measurements are considered to be approximately described by

$$t_i = \bar{t}_i + \eta_i \tag{19}$$

where η_i represents the measurement noise for receiver i (corresponds to the differential quantization error induced by the acoustic system sampling frequency and the digital implementation of the detection algorithms).

The travel time from the transponder to each receiver on the USBL array can be expressed by the following expressions

$$\bar{t}_i = \| {}^E\bar{\mathbf{p}}_t - {}^E\bar{\mathbf{p}}_i \| / v_p = \| {}^E\bar{\mathbf{p}}_t - \bar{\mathbf{p}} - \bar{\mathcal{R}}\, {}^B\bar{\mathbf{p}}_i \| / v_p \tag{20}$$

$$= \| {}^B\bar{\mathbf{p}}_t - {}^B\bar{\mathbf{p}}_i \| / v_p \tag{21}$$

where ${}^E\bar{\mathbf{p}}_i$ and ${}^B\bar{\mathbf{p}}_i$ are the positions of receiver i, respectively, in Earth and Body coordinate frames, ${}^E\bar{\mathbf{p}}_t$ is the known position of the transponder in Earth coordinate frame, and v_p represents the acoustic waves velocity underwater, assumed constant and known.

Using the approximation for the attitude error (4) and the position error definition (7) in (20) yields (see Morgado et al. [2006])

$$\bar{t}_i \approx \| {}^E\bar{\mathbf{p}}_t - \mathbf{p} + \delta\mathbf{p} - \mathcal{R}\, {}^B\bar{\mathbf{p}}_{r_i} - \left[\mathcal{R}\, {}^B\bar{\mathbf{p}}_{r_i} \times\right] \delta\boldsymbol{\lambda} \| / v_p \tag{22}$$

which are integrated into the Earth-fixed EKF as observations for each receiver by linearizing $\bar{t}_i$ about the filter state space variables and the INS estimated quantities. In this case $\delta\mathbf{p}$ represents the position error define in (7) and $\delta\boldsymbol{\lambda}$ represents the attitude error defined in (4).

The Body-fixed EKF linearizes its observations directly from (21)

$$\bar{t}_i = \| {}^B\mathbf{p}_t - \delta\mathbf{p} - {}^B\bar{\mathbf{p}}_{r_i} \| / v_p \tag{23}$$

where $\delta\mathbf{p}$ represents now the Body-fixed position error defined in (15).

3. THE POSTERIOR CRAMÉR-RAO BOUND

The Posterior Cramér-Rao Bound (PCRB) arises as a valuable analysis tool to assess the performance of dynamical estimators. It is also suitable for non-linear non-stationary dynamical systems as is the case of the work presented herein. The solution proposed in Van Trees [1968], did not allow for an efficient computation of the bound. A recursive method for an efficient computation of the PCRB for the discrete-time case was presented in Tichavsky et al. [1998]. Readers not familiarized with the theory beyond the PCRB should follow the review presented in Tichavsky et al. [1998] and references therein.

Consider the general form for the process and observation models

$$\begin{aligned} \mathbf{x}_{k+1} &= \mathbf{f}_k(\mathbf{x}_k, \mathbf{w}_k) \\ \mathbf{z}_k &= \mathbf{h}_k(\mathbf{x}_k, \mathbf{v}_k) \end{aligned} \tag{24}$$

where $\mathbf{x}_k$ is the system state at sample time k, $\{\mathbf{z}_k\}$ is the set of available measurements, $\{\mathbf{w}_k\}$ and $\{\mathbf{v}_k\}$ are independent white processes, and $\mathbf{f}_k$ and $\mathbf{h}_k$ are possibly non-linear non-stationary functions.

Let $\hat{\mathbf{x}}_k$ be any estimate of the true state vector of the process given by (24).

Since we are interested in the class of unbiased estimators for the state vector, we have the following inequality for the covariance of the estimation error

$$P_k = E\left\{ [\hat{\mathbf{x}}_k - \mathbf{x}_k] [\hat{\mathbf{x}}_k - \mathbf{x}_k]^T \right\} \geq J_k^{-1} \tag{25}$$

where J_k is the posterior Fisher Information Matrix (FIM) defined as

$$J_k = E\left\{ -\nabla_{\mathbf{x}_k} \nabla_{\mathbf{x}_k}^T \log p(\mathbf{x}_k, \mathbf{z}_k) \right\} \tag{26}$$

where $p(\mathbf{x}_k, \mathbf{z}_k)$ is the joint probability density function of the state vector and observations throughout the full extent of the trajectory of the underlying dynamical system.

Tichavsky et al. [1998] show that the FIM J_k can be efficiently computed using the following recursion

$$J_{k+1} = D_k^{22} - D_k^{21} \left(J_k + D_k^{11} \right)^{-1} D_k^{12} \tag{27}$$

where

$$D_k^{11} = E_{p(\mathbf{x}_{k+1}|\mathbf{z}_{k+1})} \left\{ -\nabla_{\mathbf{x}_k} \nabla_{\mathbf{x}_k}^T \log p(\mathbf{x}_{k+1}, \mathbf{x}_k) \right\} \tag{28}$$

$$D_k^{12} = E_{p(\mathbf{x}_{k+1}|\mathbf{z}_{k+1})} \left\{ -\nabla_{\mathbf{x}_k} \nabla_{\mathbf{x}_{k+1}}^T \log p(\mathbf{x}_{k+1}, \mathbf{x}_k) \right\} = \left[D_k^{21} \right]^T \tag{29}$$

$$D_k^{22} = E_{p(\mathbf{x}_{k+1}|\mathbf{z}_{k+1})} \left\{ -\nabla_{\mathbf{x}_{k+1}} \nabla_{\mathbf{x}_{k+1}}^T \log p(\mathbf{x}_{k+1}, \mathbf{x}_k) \right\} + E_{p(\mathbf{x}_{k+1}|\mathbf{z}_{k+1})} \left\{ -\nabla_{\mathbf{x}_{k+1}} \nabla_{\mathbf{x}_{k+1}}^T \log p(\mathbf{z}_{k+1}, \mathbf{x}_{k+1}) \right\} \tag{30}$$

and the recursion is initialized with

$$J_0 = E\left\{ -\nabla_{\mathbf{x}_0} \nabla_{\mathbf{x}_0}^T \log p(\mathbf{x}_0) \right\} \tag{31}$$

In order to compute the terms (28-30), the expected value operator $E_{p(\mathbf{x}_{k+1}|\mathbf{z}_{k+1})}\{\cdots\}$ needs to be evaluated. The computational complexity of these expectations depends entirely on the structure of the underlying process and observation models, and involves solving integral terms that, in general, do not have closed-form solutions, neither in the particular case of the estimators presented herein. As suggested in Šimandl et al. [2001], the terms can be estimated using Monte-Carlo simulations and replacing the expected values by the sample mean of the realizations, e.g. the term (28) is computed as

$$\hat{D}_k^{11} = \frac{1}{M} \sum_{j=1}^{M} -\nabla_{\mathbf{x}_k} \nabla_{\mathbf{x}_k}^T \log p(\mathbf{x}_{k+1}, \mathbf{x}_k) \big|_{\mathbf{x}_k = \mathbf{x}_k(j)} \tag{32}$$

where $\{\mathbf{x}_k(j)\}_{k=0}^N$ is the jth realization of the state trajectory, $j = 1, 2, \ldots, M$, and M is the number of Monte-Carlo realizations. As expected, as M increases the quality

of the Monte-Carlo estimates improve, however there is no rule of thumb on selecting an M that guarantees that the estimates will be satisfactory.

In the scope of the work presented herein, we restrict the PCRB evaluation to the discrete-time Additive White Gaussian Noise (AWGN) case in which comes for the process and observation models

$$\begin{aligned} \mathbf{x}_{k+1} &= \mathbf{f}_k(\mathbf{x}_k) + \mathbf{w}_k \\ \mathbf{z}_k &= \mathbf{h}_k(\mathbf{x}_k) + \mathbf{v}_k \end{aligned} \tag{33}$$

where now $\mathbf{x}_k$ represents the discretized errors of the navigation systems at sample time k, as presented in Section 2, $\{\mathbf{w}_k\}$ is the process equivalent AWGN, $\{\mathbf{v}_k\}$ is the measurement equivalent AWGN, $\{\mathbf{z}_k\}$ is the set of available measurements which are related to the state vector by the non-linear non-stationary observation function $\mathbf{h}_k$, and $\mathbf{f}_k$ models the discretized navigation system error model.

In this framework, the logarithmic terms of the PCRB recursion can be written as

$$-\log p(\mathbf{x}_{k+1}, \mathbf{x}_k) = c_1 + \frac{1}{2}[\mathbf{x}_{k+1} - \mathbf{f}_k(\mathbf{x}_k)]^T Q_k^{-1}[\mathbf{x}_{k+1} - \mathbf{f}_k(\mathbf{x}_k)] \tag{34}$$

$$-\log p(\mathbf{z}_{k+1}, \mathbf{x}_{k+1}) = c_2 + \frac{1}{2}[\mathbf{z}_{k+1} - \mathbf{h}_{k+1}(\mathbf{x}_{k+1})]^T R_{k+1}^{-1}[\mathbf{z}_{k+1} - \mathbf{h}_{k+1}(\mathbf{x}_{k+1})] \tag{35}$$

where c_1 and c_2 are constants, Q_k is the discrete equivalent process AWGN covariance matrix, and R_k is the discrete equivalent observation AWGN covariance matrix.

Thus, it can be easily derived for the terms (28-30)

$$D_k^{11} = E\left\{\mathbf{F}_k^T(\mathbf{x}_k) Q_k^{-1} \mathbf{F}_k(\mathbf{x}_k)\right\} \tag{36}$$

$$D_k^{12} = -E\left\{\mathbf{F}_k^T(\mathbf{x}_k)\right\} Q_k^{-1} \tag{37}$$

$$D_k^{22} = Q_k^{-1} + E\left\{\mathbf{H}_{k+1}^T(\mathbf{x}_{k+1}) R_{k+1}^{-1} \mathbf{H}_{k+1}(\mathbf{x}_{k+1})\right\} \tag{38}$$

where

$$\mathbf{F}_k(\mathbf{x}_k) = [\nabla_{\mathbf{x}_k} \mathbf{f}_k^T]^T \tag{39}$$

$$\mathbf{H}_{k+1}(\mathbf{x}_{k+1}) = [\nabla_{\mathbf{x}_{k+1}} \mathbf{h}_{k+1}^T]^T \tag{40}$$

are the Jacobians of $\mathbf{f}_k$ and $\mathbf{h}_{k+1}$, respectively, evaluated at their true values.

To correctly compute the PCRB for specific navigation systems in analysis herein, the numerical integration algorithms are executed in a direct-feedback setting without the EKF in the loop, for M Monte-Carlo realizations of the inertial sensors AWGN. In each integration step the errors that arise from the inertial algorithms are recorded for posterior evaluation of the PCRB and corrected in the correction routines maintaining the linearization assumptions valid. Using this setup the evaluated PCRB assesses the attainable performance of any estimator that is placed in the direct-feedback loop.

4. SIMULATION RESULTS

The overall navigation system performance was assessed in simulation. The USBL array is composed of five hydrophones installed on the vehicle, for instance on the nose cone, according to the configuration depicted in Fig. 3. The maximum distance between the receivers is 20 cm, which are mounted on a non coplanar configuration. The pinger on the vehicle interrogates the transponder every second, leaving enough time after the reception of the reply for disturbance phenomena like multi-path to fadeout on the channel.

The Time-Of-Arrival (TOA) of the acoustic waves arriving at the receivers are considered to be disturbed by zero mean Additive White Gaussian Noise (AWGN) with a variance of $(2500\mu s)^2$ prior to the quantization procedure (note that this AWGN is the same for all receivers and that the differential disturbance is induced by the quantization). The acoustic quantization was performed with a sampling frequency of 400 kHz.

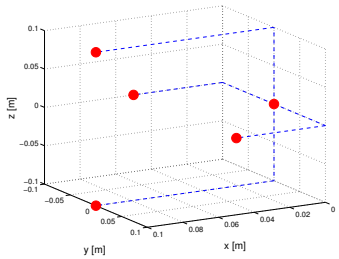

Fig. 3. Receivers installation geometry

The INS provides measurements of the position, velocity and attitude with a frequency of 50 Hz. The white Gaussian noise and bias characteristics of the sensors are presented in Table 1. A magnetometer is also used in the proposed solutions, as presented in Morgado et al. [2006], yielding attitude estimation improvements. The noise and bias characteristics used in the simulations are inspired on the Crossbow CXL10TG3 triaxial accelerometer, the Crossbow CXM113 triaxial magnetometer, and on the Silicon Sensing Systems CRS03 triaxial rate gyro.

Table 1. Sensor characteristics

Sensor	**Bias**	**Standard Deviation - σ**
Rate gyro	5 °/s	0.05 °/s
Accelerometer	12 mg	0.6 mg
Magnetometer	(Calibrated)	60 μG

The performance of both estimators is assessed resorting to Monte-Carlo simulations over the same trajectory and the same set of noise realizations. The PCRB of both systems is also computed using 500 runs of Monte-Carlo simulations as described in Sec. 3. In the results presented herein, the output of the Body-fixed estimator is converted to the same representation of the Earth-fixed estimator and vice-versa for performance comparison purposes.

The vehicle describes a path composed of several tight curves, as illustrated in Fig. 4, in order to achieve high angular velocities and to fully extent the differences between the two models. All inertial sensors have an initial bias misalignment of 1/3 on all axis. The acoustic transponder is placed 200 meters away, in the x coordinate, from the initial position of the vehicle.

The Root-Mean-Square (RMS) error in position of both systems, based on a Monte-Carlo simulation of 100 runs, is plotted in Fig. 5 and represented in Earth-fixed coordinates. This plot also displays the PCRB of the Earth-fixed system and the covariance estimate of the filter designed in Earth-fixed coordinates. An analogous plot is presented in Fig. 6 with a view from Body-fixed coordinate frame.

Surprisingly enough, as it can be seen from the figures, the performance of the estimators designed in the two different coordinates, Earth-fixed and Body-fixed, is equivalent across representation frames for this class of systems. In fact, the black line in the graphs that represents the Earth-fixed estimator output error is not distinguishable from the

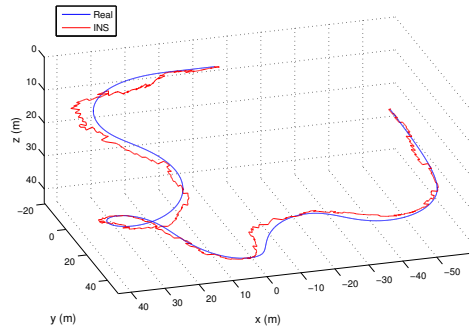

Fig. 4. Vehicle trajectory and Earth-fixed system output

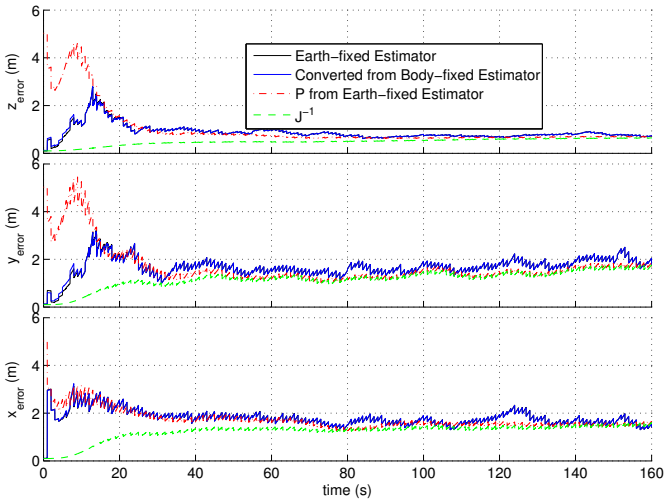

Fig. 5. Position RMS error Earth-fixed coordinate frame

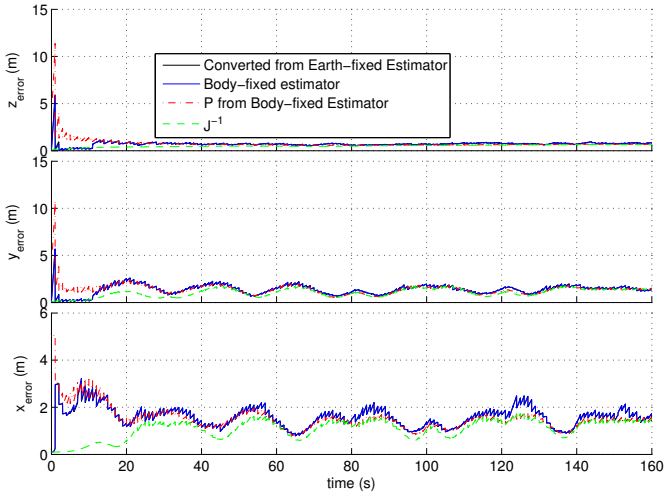

Fig. 6. Position RMS error Body-fixed coordinate frame

blue one because of this performance equivalence. From an analysis of the results it becomes also clear that, in the conditions presented herein, the estimators perform very close to the lower bound provided by the PCRB in both coordinate frames. After an initial transient due to the bias misalignment in the inertial sensors it can be seen that the filter estimates converge to the PCRB along the described trajectory. Comparing the estimated covariance of the EKF with the RMS of the position error it can also be seen that the filters are as expected coherent.

5. CONCLUSIONS AND FUTURE WORK

The work presented in this paper addressed the performance analysis of USBL aided INS's and the methodologies that can be used to optimally design these class of systems on different coordinate frames, in particular on Earth-fixed and on Body-fixed coordinate frames. The performance of the navigation systems designed in these two coordinate frames was compared in simulation resorting to Monte-Carlo simulations and shown to be equivalent. The results presented herein also revealed that the performance of both systems is close to the lower bound provided by the PCRB. Future work on this subject will have its main focus on the implementation and field validation of the proposed techniques on board the underwater vehicles operated by ISR.

REFERENCES

K.R. Britting. *Inertial Navigation Systems Analysis*. John Wiley & Sons, Inc., 1971.

E. Hairer, S. P. Nrsett, and Gerhard Wanner. *Solving ordinary differential equations*. Springer series in computational mathematics ;. Springer-Verlag, Berlin ; New York, 2nd rev. edition, 1993. E. Hairer, S.P. Nrsett, G. Wanner.ill. ; 25 cm. 1. Nonstiff problems.

M.B. Larsen. Synthetic long baseline navigation of underwater vehicles. In *Proceedings of the MTS/IEEE TECHNO-OCEAN Oceans'04 Conference*, volume 3, pages 2043–2050, Providence, RI, USA, September 2000.

P.M. Lee, B.H. Jeon, S.M. Kim, H.T. Choi, C.M. Lee, T. Aoki, and T. Hyakudome. An integrated navigation system for autonomous underwater vehicles with two range sonars, inertial sensors and Doppler velocity log. In *Proceedings of the MTS/IEEE TECHNO-OCEAN Oceans'04 Conference*, volume 3, pages 1586–1593, Kobe, Japan, November 2004.

X. Lurton and N.W. Millard. The feasibility of a very-long baseline acoustic positioning system for AUVs. In *Proceedings of the IEEE OCEANS '94 Conference*, volume 3, pages 403–408, Brest, France, September 1994.

P.H. Milne. *Underwater Acoustic Positioning Systems*. Gulf Pub. Co., 1983.

M. Morgado, P. Oliveira, C. Silvestre, and J.F. Vasconcelos. USBL/INS Tightly-Coupled Integration Technique for Underwater Vehicles. In *Proceedings Of The 9th International Conference on Information Fusion*, Florence, Italy, July 2006. IEEE.

A. Pascoal, P. Oliveira, and C. Silvestre *et al.* Robotic Ocean Vehicles for Marine Science Applications: the European ASIMOV Project. In *Proceedings of the Oceans 2000*, Rhode Island, USA, September 2000.

K.M. Roscoe. Equivalency Between Strapdown Inertial Navigation Coning and Sculling Integrals/Algorithms. *AIAA Journal of Guidance, Control, and Dynamics*, 24(2):201–205, 2001.

P.G. Savage. Strapdown Inertial Navigation Integration Algorithm Design Part 1: Attitude Algorithms. *AIAA Journal of Guidance, Control, and Dynamics*, 21(1):19–28, January-February 1998a.

P.G. Savage. Strapdown Inertial Navigation Integration Algorithm Design Part 2: Velocity and Position Algorithms. *AIAA Journal of Guidance, Control, and Dynamics*, 21(2):208–221, March-April 1998b.

S.M. Smith and D. Kronen. Experimental results of an inexpensive short baseline acoustic positioning system for AUV navigation. In *Proceedings of the MTS/IEEE Oceans'97 Conference*, volume 1, pages 714–720, Halifax, Nova Scotia, Canada, October 1997.

P. Tichavsky, C. H. Muravchik, and A. Nehorai. Posterior Cramér - Rao bounds for discrete-time nonlinear filtering. *Signal Processing, IEEE Transactions on*, 46(5):1386–1396, 1998.

HL Van Trees. *Detection, estimation, and modulation theory.. part 1,. detection, estimation, and linear modulation theory*. Wiley New York, 1968.

K. Vickery. Acoustic positioning systems. New concepts - The future. In *Proceedings Of The 1998 Workshop on Autonomous Underwater Vehicles, AUV'98*, Cambridge, MA, USA, August 1998.

M Šimandl, J Krlovec, and P Tichavsk. Filtering, predictive, and smoothing Cramér Rao bounds for discrete-time nonlinear dynamic systems. *Automatica*, 37(11):1703–1716, 2001.